



OPEN ACCESS

EDITED BY

Chen Ling,
Toyota, United States

REVIEWED BY

Utsav Raj Aryal,
Toyota Research Institute, United States
Yongxiao Tuo,
China University of Petroleum, China

*CORRESPONDENCE

Yao Yao,
✉ yyaoak@connect.ust.hk
Haijiang Wang,
✉ wanghj@sustech.edu.cn

RECEIVED 12 April 2023

ACCEPTED 24 May 2023

PUBLISHED 07 June 2023

CITATION

Yao K, Long T, Wang Y, Yuan X-Z, Yao Y
and Wang H (2023), Measuring the
through-plane and in-plane oxygen
apparent diffusion coefficients in the gas
diffusion layer.
Front. Energy Res. 11:1200603.
doi: 10.3389/fenrg.2023.1200603

COPYRIGHT

© 2023 Yao, Long, Wang, Yuan, Yao and
Wang. This is an open-access article
distributed under the terms of the
[Creative Commons Attribution License
\(CC BY\)](https://creativecommons.org/licenses/by/4.0/). The use, distribution or
reproduction in other forums is
permitted, provided the original author(s)
and the copyright owner(s) are credited
and that the original publication in this
journal is cited, in accordance with
accepted academic practice. No use,
distribution or reproduction is permitted
which does not comply with these terms.

Measuring the through-plane and in-plane oxygen apparent diffusion coefficients in the gas diffusion layer

Keguang Yao^{1,2}, Tiehan Long³, Yajun Wang⁴, Xiao-Zi Yuan⁵,
Yao Yao^{2*} and Haijiang Wang^{2,6*}

¹School of Materials Science and Engineering, Harbin Institute of Technology, Harbin, Heilongjiang, China, ²Department of Mechanical and Energy Engineering, Southern University of Science and Technology, Shenzhen, Guangdong, China, ³China Academy of Aerospace Aerodynamics, Beijing, China, ⁴School of Electrical Engineering, University of South China, Hengyang, China, ⁵Energy, Mining and Environment Research Center, National Research Council Canada, Vancouver, BC, Canada, ⁶Key Laboratory of Energy Conversion and Storage Technologies, Southern University of Science and Technology, Shenzhen, China

Accurately predicting oxygen mass transport resistance and current distribution in fuel cells requires significant knowledge of oxygen diffusion coefficients in both in-plane and through-plane directions. However, there are few methods for measuring in-plane oxygen diffusion coefficients, which are important parameters for simulating oxygen flux distribution in gas diffusion layers (GDLs). In this study, we establish measurement methods and calculations for both in-plane and through-plane oxygen diffusion coefficients. Using in-house designed cells, we measure the in-plane and through-plane oxygen apparent diffusion coefficients of a commercial carbon paper (AvCarb EP40) at various torques and gas flow rates. We also simulate oxygen flux distributions in the GDL under each torque and gas flow rate. Our results show that the channel part is the major contributor to total oxygen flux at high torque conditions and that an increase in torque leads to a decrease in the contribution from the land part. Simulation results also suggest that a higher gas flow rate and lower torque contribute to a more uniform distribution of oxygen flux in the GDL.

KEYWORDS

proton exchange membrane fuel cells, gas diffusion layer, oxygen diffusion coefficients, land, channel

1 Introduction

Proton exchange membrane fuel cell (PEMFC) is an attractive technology for converting the chemical energy of hydrogen to electricity, offering advantages such as zero toxic gas and CO₂ emissions, high energy efficiency, and compatibility with alternative/renewable energy sources (Curtin et al., 2004). However, further cost reduction and performance improvement are necessary for commercial applications. One promising approach is to increase the operating current density, typically higher than 2 A/cm² (Ahmed and Sung, 2006; Chan et al., 2012; Ozden et al., 2019). However, under such high current density conditions, reactant mass transport and water flooding in the gas diffusion layer (GDL) become major limitations. The GDL, usually made of carbon paper or carbon cloth and treated with a hydrophobic agent such as polytetrafluoroethylene (PTFE), is a sub-component of the membrane electrode assembly (MEA) in PEMFC. It serves as a link between the flow field

and catalyst layer (Omrani and Shabani, 2019; Ozden et al., 2019) and serves multiple functions, including electrical contact, heat conduction, structural support, water management, and uniform gas distribution (Williams et al., 2004; Dai et al., 2008).

The apparent diffusion coefficient is a crucial parameter for evaluating how quickly gas or vapor products/reactants can pass through the porous structure of the GDL. Its apparent diffusion coefficient plays an essential role in assessing gas mass transport at high current densities. In PEMFCs, the relatively low diffusivity of oxygen than that of hydrogen is the primary limitation at high current density conditions (Ozden et al., 2019). Hence, accurate measurement of the apparent diffusion coefficient, particularly the oxygen apparent diffusion coefficient in the GDL, is critical for predicting mass transport resistance in fuel cells and enabling more precise simulations of PEMFCs.

Previous studies have employed *in situ* limiting current techniques (Williams et al., 2004; Stumper et al., 2005; Baker et al., 2006) in PEMFCs or *ex situ* techniques (Rohling et al., 2007; Astrath et al., 2009; Zamel et al., 2010; Shen et al., 2011; Chan et al., 2012) involving a Loschmidt cell to measure the oxygen diffusion coefficient. The *in situ* limiting current technique is a simple and rapid method for measuring the average mass transport resistance in PEMFCs which determines the relationship between the measured limiting current and the oxygen effective diffusion coefficient in the cathode. Using this technique, Beuscher (2006) found that the gas diffusion media in PEMFCs contribute only 26% to the total mass transport resistance, with Knudsen diffusion and film diffusion through ionomer and water film constituting the majority of the mass transport resistance.

Loschmidt cells are widely employed as an *ex situ* technique for measuring the GDL gas diffusion coefficient. Chan et al. (2012) used a modified Loschmidt cell to study the impact of the microporous layer (MPL) on the oxygen diffusion coefficient in the GDL. They discovered that the effective diffusion coefficient of the MPL accounts for only 21% of that of the GDL substrate, with Knudsen diffusion representing the majority of diffusion in the MPL. Furthermore, Zamel et al. (2010) employed experimental measurements in a Loschmidt cell to demonstrate that the existing theoretical models overpredicted the effective diffusion coefficient about four- to fivefold, leading to an underestimation of the mass transport limitation. Additionally, studies have explored the effects of relative humidity (Astrath et al., 2009), PTFE content (Fluckiger et al., 2008), compression (Kramer et al., 2008; LaManna and Kandlikar, 2011; Rashapov et al., 2015; Khetabi et al., 2019), and thickness (LaManna and Kandlikar, 2011) on the effective diffusion coefficient.

This study establishes methods for measuring both the in-plane and through-plane oxygen apparent diffusion coefficients, while taking into account the impact of gas flow rates and torques—closer to the real conditions experienced by fuel cells than the pure diffusion usually studied. Furthermore, we also simulate the effects of gas flow rates and torques on the oxygen concentration distribution in the GDL.

2 Experimental setup

The cathode of a fuel cell comprises the bipolar plate, gas diffusion layer (GDL), and catalyst layer (Scheme 1). The land

and channel are both essential parts of the bipolar plate, serving to conduct the current and distribute the reactant gas, respectively. Consequently, the GDL in the cathode can be divided into two parts, namely, the channel and the land parts, located on the channel and land of the bipolar plate, respectively. The GDL's main function is to ensure the uniform distribution of gas reactants to the catalyst layer. In the channel part, oxygen gas diffuses through the GDL to reach the catalyst layer. However, in the land area, both in-plane and through-plane diffusion affect oxygen distribution in the GDL.

The relationship between the reactant gas flux and the gas diffusion coefficient can be obtained according to Fick's First Law (Eq. 1), noting that j_{flux} is the flux of the reactant gas, D is the gas apparent diffusion coefficient, dc is the change in concentration, and dx is the change in distance.

$$j_{flux} = -D \left(\frac{dc}{dx} \right). \quad (1)$$

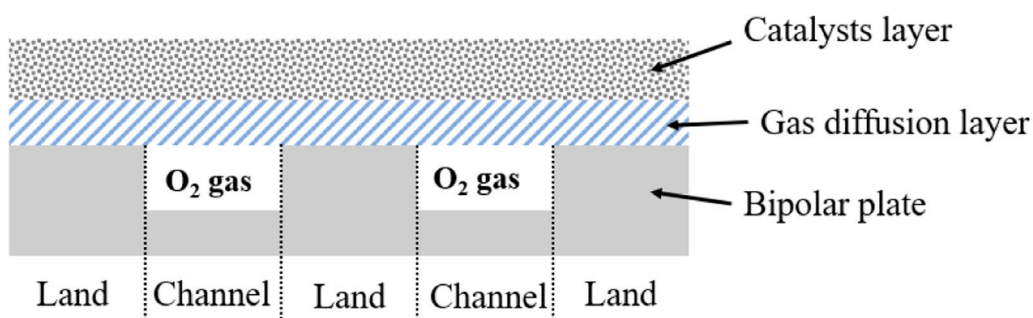
2.1 Experimental apparatus for in-plane apparent diffusion coefficient measurements

To measure the in-plane diffusion coefficient, we designed a diffusion cell (Scheme 2A and Scheme 2B). The cell comprises two chambers, A and B, separated by a carbon paper (AvCarb EP40) GDL with a width of 10 mm. Each chamber has a length of 92 mm and a depth of 8 mm. To control the gas flow rates, nitrogen and oxygen mass flow controllers (Qixinghuachuang, CS200) are connected to the inlet valves (valves 1 and 3). Valves 2 and 4 serve as gas outlets. Oxygen concentration changes in the chambers are measured using oxygen mini-sensors (PyroScience, OXF500PT) connected to an oxygen meter (PyroScience, FSO2-4). The sensors are placed in the middle of the edge of chambers A and B, as shown in Scheme 2A and Scheme 2B.

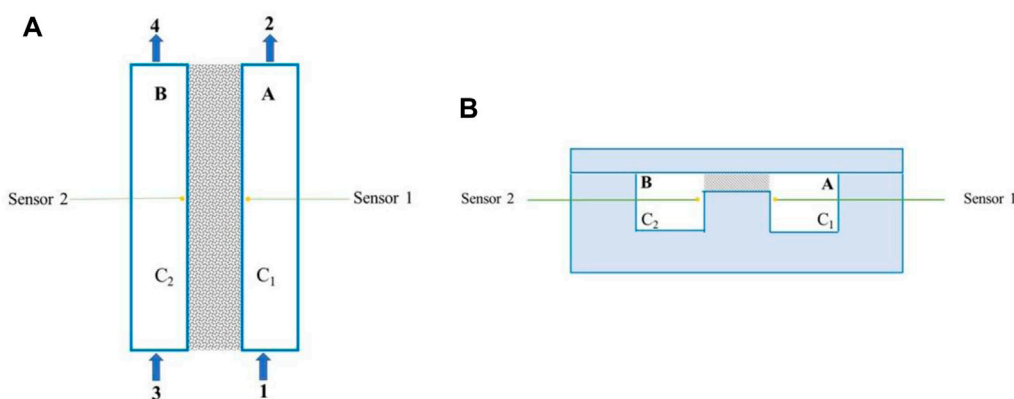
Before conducting the measurements, nitrogen gas is flowed into chambers A and B at a rate of 200 ccm for 30 min via valves 1 and 3 to remove oxygen from the setup, until the oxygen meter reading approaches 0. Valves 3 and 4 are then closed, and a mixture of nitrogen and oxygen (1:1) is introduced into Chamber A through Valve 1 at varying total flow rates (200–2000 ccm). Simultaneously, oxygen mini-sensors 1 and 2 record the readings, producing the C-t curves depicted in Figure 1A. In this case, the increase in the amount of O₂ in Chamber B is equal to the amount flowing through the GDL, as indicated in Eq. 2, where V_B is the volume of Chamber B, L is the width of the land, A is the sectional area of the GDL during the test, $D_{H, apparent}$ is the in-plane oxygen apparent diffusion coefficient at a constant gas flow rate, and C_1 and C_2 represent the oxygen concentrations in Chambers A and B, respectively.

$$\frac{dC_2}{dt} \times V_B = D_{H, apparent} \times \left(\frac{C_1 - C_2}{L} \right) \times A. \quad (2)$$

By combining the C-t curves and Eq. 2, the relationship between dC_2/dt and $C_1 - C_2$ at each moment could be collected, as shown in Figure 1B. Then, the in-plane oxygen apparent diffusion coefficient ($D_{H, apparent}$) under a constant flow rate can be calculated with the known values of the slope of the fitting line, section area A , and the volume of Chamber B, based on Eq. 2.



SCHEME 1
Configuration of bipolar plate, gas diffusion layer, and catalyst layer in the PEMFC cathode.



SCHEME 2
(A) Top view and (B) cross-sectional view of the schematic diagram of the diffusion cell for in-plane oxygen apparent diffusion efficiency measurements (gray area is the GDL).

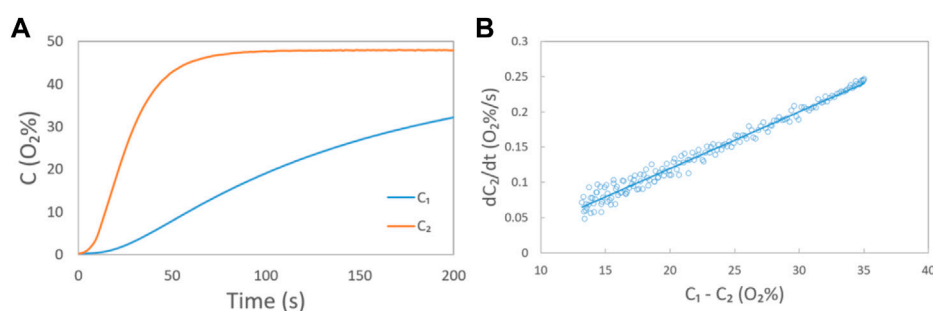
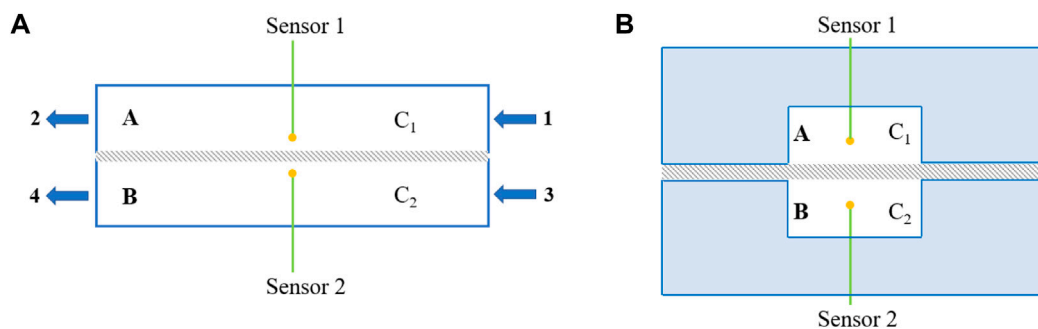


FIGURE 1
(A) Oxygen concentration in chambers A and B in Scheme 2 measured by oxygen sensors 1 and 2, respectively, at a gas mixture ($O_2: N_2 = 1:1$) flow rate of 200 ccm. In this case, chambers A and B are separated by a slit filled with nitrogen (width: 10 mm, depth: 0.3 mm); (B) relationship between dC_2/dt and $C_1 - C_2$ at each moment (circle) and the corresponding fitted line (solid line) at a gas flow rate of 200 ccm.

2.2 Experimental apparatus for through-plane diffusion coefficient measurements

Scheme 3A and Scheme 3B show the setup used to measure the through-plane apparent diffusion coefficient of oxygen. The

diffusion cell consisted of chambers A and B separated by a GDL made of AvCarb EP40 carbon paper with a width of 10 mm. The gas flow rates were controlled by oxygen and nitrogen mass flow controllers (Qixinghuachuang, CS200) connected to the inlet (valves 1 and 3). The gas outlets were valves 2 and 4. Oxygen



SCHEME 3
 (A) Side view and (B) cross-sectional view of the schematic diagram of the diffusion cell for oxygen through-plane apparent diffusion efficiency measurements (gray area is the GDL).

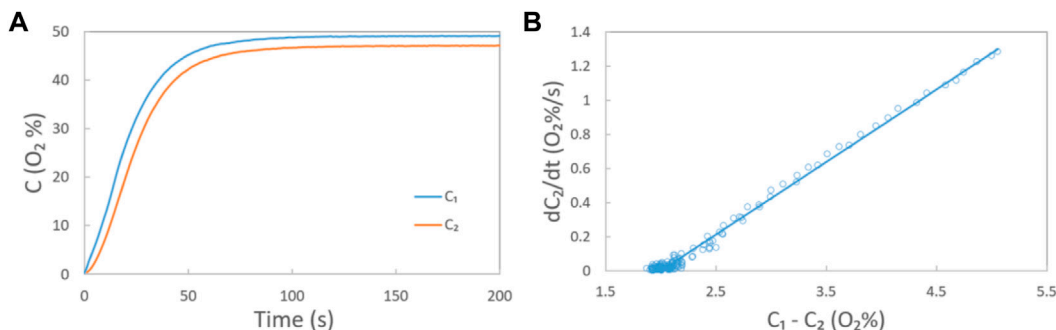


FIGURE 2
 (A) Oxygen concentration in chambers A and B in Scheme 3 measured by oxygen sensors 1 and 2, respectively, at a gas mixture (O₂: N₂ = 1:1) flow rate of 200 ccm. In this case, chambers A and B are separated by a carbon paper GDL (AvCarb EP40); (B) relationship between dC_2/dt and $C_1 - C_2$ at each moment (circle) and the corresponding fitted (solid) line during the oxygen through-plane apparent diffusion coefficient measurements.

mini-sensors (PyroScience, OXF500PT) were placed in chambers A and B and connected to an oxygen meter (PyroScience, FSO2-4) to measure the oxygen concentration change in the chambers. The distance between the tips of oxygen sensors 1 and 2 was 5.21 mm.

Like the measurement of the oxygen in-plane apparent diffusion coefficient, the setup was purged with nitrogen gas flowing in Chambers A and B at a rate of 200 ccm for 30 min through Valves 1 and 3 to remove oxygen before the measurements. The oxygen meter reading was closely monitored and stabilized at 0. Once stabilized, gas outlet Valves 3 and 4 were closed, and a mixture of nitrogen and oxygen (1:1) flowed into Chamber A through Valve 1 at various flow rates (200–2,000 ccm). Oxygen mini-sensors 1 and 2 were used to simultaneously record the C-t curves (Figure 2A). Both the impact of in-plane and through-plane diffusion coexist in Scheme 3. However, considering that the concentration difference in the in-plane direction is negligible for the high gas flow rates (200–2000 ccm) in this direction, the impact of in-plane diffusion is neglected here. In this case, the increase in the amount of O₂ in Chamber B was equal to the amount flowing through the GDL, as demonstrated by Eq. 3, where V_B (5.6 cm³) represents the volume of Chamber B, L (0.521 cm) represents the distance between oxygen mini-sensors 1 and 2, A (8 cm²) represents

the sectional area of the GDL during the test, $D_{V, apparent}$ represents the apparent oxygen through-plane diffusion coefficient, and C_1 and C_2 represent the oxygen concentrations in Chambers A and B, respectively.

$$\frac{dC_2}{dt} \times V_B = D_{V, apparent} \times \left(\frac{C_1 - C_2}{L} \right) \times A. \quad (3)$$

By combining the C-t curves in Figure 2A and Eq. 3, the relationship between dC_2/dt and $C_1 - C_2$ at each moment could be recorded (Figure 2B). Then, the apparent oxygen through-plane diffusion coefficient $D_{V, apparent}$ under each gas flow rate could be calculated with known values of the slope of the fitting line, the section area A , and the volume of Chamber B, based on Eq. 3.

3 Results and discussion

To validate the measurements and the calculation, the oxygen apparent diffusion coefficient in nitrogen gas was measured with the diffusion cell shown in Scheme 2A and Scheme 2B, where chambers A and B are separated by a slit filled with nitrogen (width: 10 mm, depth: 0.3 mm). Figures 3A,B show the oxygen concentration (C_1

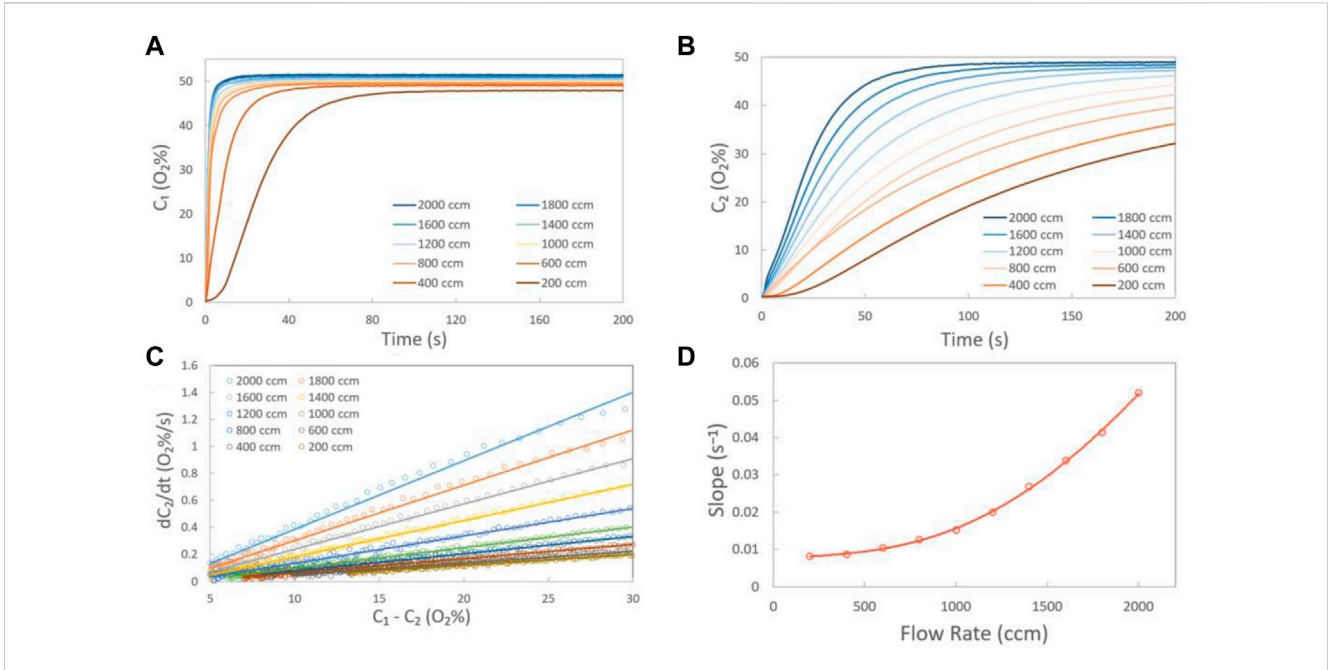


FIGURE 3 Oxygen concentrations in chambers A (A) and B (B) at various gas mixture (O₂: N₂ = 1:1) flow rates; (C) measured data (circle) at various gas flow rates and the corresponding fitting (solid) lines by Eq. 2; (D) value of the slope under various flow rates (circle) and the fitted (solid) line. In this case, chambers A and B of the diffusion cell for in-plane oxygen diffusion efficiency measurement are separated by a slit filled with nitrogen (width: 10 mm, depth: 0.3 mm).

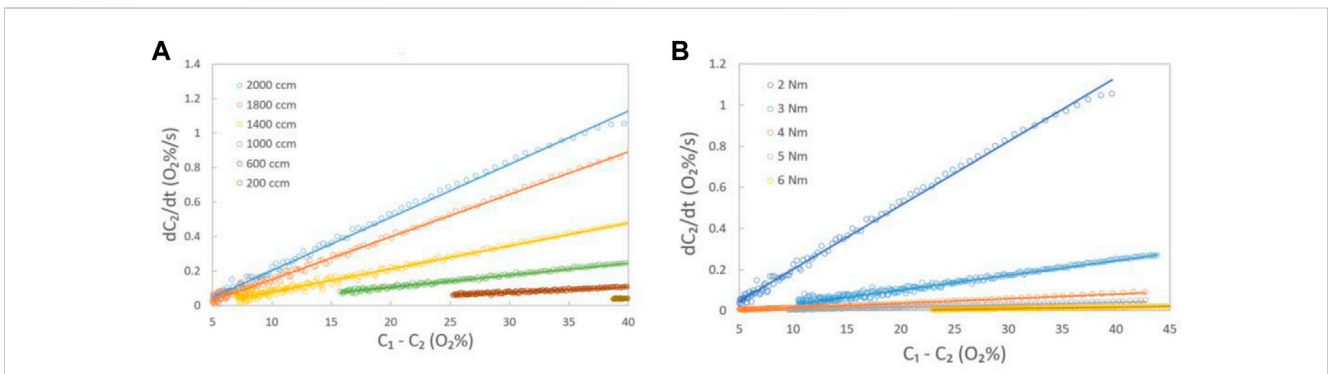


FIGURE 4 (A) Measured data (circle) at various gas flow rates and the corresponding fitting (solid) lines by Eq. 2 at a torque of 2 Nm; (B) Measured data (circle) at a gas flow rate of 2,000 ccm and the corresponding fitting (solid) lines by Eq. 2 at various torques in the in-plane diffusion cell.

and C₂) in Chambers A and B at various gas flow rates, respectively. The linear relationship between dC₂/dt and C₁-C₂ at various inlet gas flow rates is given in Figure 3C. Based on Eq. 2 and Figure 3C, the slope of dC₂/dt and C₁-C₂ which is the value of D_H×A/V_B at various flow rates could be calculated. The result is given in Figure 3D, as well as the fitted line with an expression of y = a×x⁴+b×x³+c×x²+d×x + e. The values of a, b, c, d, and e are -2 × 10⁻¹⁵, 1 × 10⁻¹¹, -4 × 10⁻⁹, 4 × 10⁻⁶, and 0.00746, respectively. At a flow rate of 0, the value of D_H×A/V_B is 0.00746, where V_B is 7.36 cm³, L is 1 cm, and A is 0.27 cm². Based on Eq. 2, D_H could be calculated as 0.203 cm²/s, very close to that of D_{N₂-O₂} (0.208 cm²/s) (Marrero and Mason, 1972),

indicating that the measurement and the calculation in this work are reliable.

Figure 4A presents the measured data and corresponding fitting lines obtained using Eq. 2 at a torque of 2 Nm under various gas flow rates. The corresponding in-plane oxygen apparent diffusion coefficients were calculated by collecting the slopes of the fitting lines and using Eq. 2, where V_B is 7.36 cm³, L is 1 cm, and A is 0.1945 cm². The in-plane oxygen apparent diffusion coefficients for each condition are listed in Table 1. Similar measurements and fitting were performed under torques of 3 Nm, 4 Nm, 5 Nm, and 6 Nm (Figure 4B). The results indicate that increasing the torque leads to a decrease in the in-plane oxygen diffusion coefficient, particularly due to a decrease in porosity.

TABLE 1 Value of $D_{H, apparent}$ under each test condition (Unit: cm^2/s).

(ccm)	2 Nm	3 Nm	4 Nm	5 Nm	6 Nm
200	0.06281	0.03519	0.02649	0.0238	0.02074
400	0.08628	0.04125	0.02812	0.0252	0.02104
600	0.12033	0.04995	0.03163	0.02486	0.02104
800	0.18201	0.06357	0.03542	0.02592	0.02142
1,000	0.26639	0.07417	0.03776	0.02933	0.02157
1,200	0.36553	0.09119	0.04314	0.03247	0.02225
1,400	0.50062	0.11201	0.04881	0.03659	0.02373
1,600	0.67885	0.14039	0.05676	0.03935	0.02342
1,800	0.90513	0.18201	0.06206	0.042	0.02547
2,000	1.17039	0.2698	0.09082	0.05298	0.02547

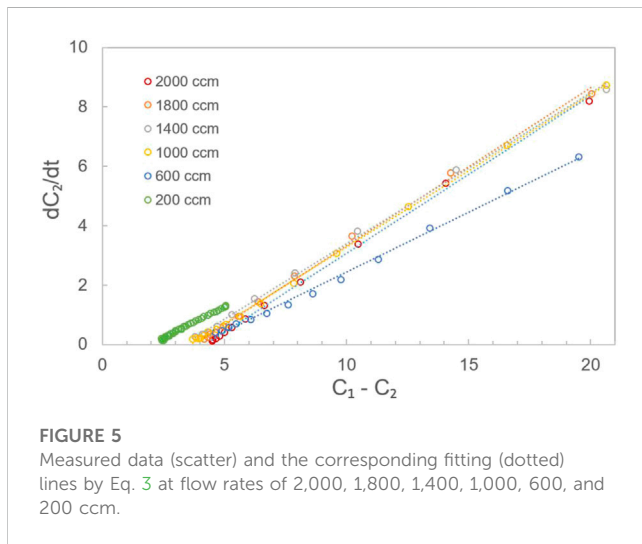


FIGURE 5 Measured data (scatter) and the corresponding fitting (dotted) lines by Eq. 3 at flow rates of 2,000, 1,800, 1,400, 1,000, 600, and 200 ccm.

The oxygen through-plane apparent diffusion coefficient of the carbon paper was measured using a through-plane diffusion cell. Figure 5 shows the measured data and the corresponding fitting line using Eq. (3) at various flow rates. The through-plane oxygen diffusion coefficient was calculated based on the slope of the fitting line in Figure 5 and Eq. 3, where V_B is 5.6 cm^3 and A is 8 cm^2 . The through-plane oxygen diffusion coefficients ($D_{V, apparent}$) of the carbon paper under various gas flow rates were calculated using Eq. (4); these are impacted by both the oxygen diffusion in nitrogen ($L = 0.5 \text{ cm}$) and the oxygen through-plane diffusion in carbon paper ($L = 0.021 \text{ cm}$), and are given in Table 2.

$$\frac{0.521}{D_{overall}} = \frac{0.5}{D_{N_2-O_2}} + \frac{0.021}{D_{V,apparent}} \quad (4)$$

3.1 Numerical simulations

To further investigate the influence of $D_{V, apparent}$ and $D_{H, apparent}$ on the oxygen distribution in GDL, the oxygen diffusion process is

TABLE 2 Value of D_{total} and $D_{V, apparent}$ at each test condition.

Flow rate (ccm)	200	600	1,000	1,400	1,800	2,000
$D_{overall}$ (cm^2/s)	0.1596	0.1449	0.1868	0.1871	0.1961	0.1935
$D_{V, apparent}$ (cm^2/s)	0.0244	0.0176	0.0545	0.0552	0.0830	0.0727

numerically simulated. The governing equation of the oxygen diffusion process without convection is

$$\frac{\partial c}{\partial t} = D_{H,apparent} \frac{\partial^2 c}{\partial x^2} + D_{V,apparent} \frac{\partial^2 c}{\partial y^2} \quad (5)$$

In which x denotes the in-plane direction, y denotes the through-plane direction, and c is local oxygen concentration at the location (x, y) . In an equilibrium state, the oxygen concentration c does not change with time. Thus, Eq. 5 can be expressed as

$$D_{H,apparent} \frac{\partial^2 c}{\partial x^2} + D_{V,apparent} \frac{\partial^2 c}{\partial y^2} = 0 \quad (6)$$

Eq. (6) is discretized with the five-point central difference scheme. The simulation region is plotted schematically in Figure 6A. On the surface of the catalyst layer, the chemical reaction rate is assumed to be oxygen mass transfer limited, and the boundary condition is thus $c = 0$. The boundary condition is $\partial c / \partial y = 0$ on the land surface and $c = 1$ in the channel. The periodic boundary condition is adopted at the left and right boundaries of the simulation region.

A total of 11 cases were conducted to present the distribution of oxygen concentration. The corresponding numerical conditions are listed in Table 3. Considering that both the porosity and the thickness of GDL in the land part would be impacted by the torques, the accurate measurements of the $D_{V, apparent}$ of the GDL in the land part would be very complex. Here, we simply assume that the $D_{V, apparent}$ and the thickness of GDL in the land part are not impacted by the torques as cases 7–11 in Table 2 show. Grid 1 (401×85) with a space interval of 0.0025 mm and grid 2 (801×169) with a space interval of 0.00125 mm are adopted simultaneously for case 1. Distributions of oxygen concentration along the in-plane middle line (from $x = 0$ to $x = 1 \text{ mm}$ at $y = 0.125 \text{ mm}$) are plotted in Figure 6B. The discrepancy between the results of grids 1 and 2 is less than 1%. Therefore, the numerical simulation result is grid-independent and grid 1 is adopted for numerical simulations in all cases to reduce computation consumption.

3.2 Numerical simulation results and discussion

Figure 7 shows the simulation results under various gas flow rates in a GDL unit with $\delta_c = 0.5 \text{ mm}$ and $\delta_L = 0.5 \text{ mm}$, respectively. As the gas flow rates decrease, the diffusion of oxygen in the land part becomes more challenging, resulting in a reduction of the amount of oxygen amount in this area. Figure 8 shows the

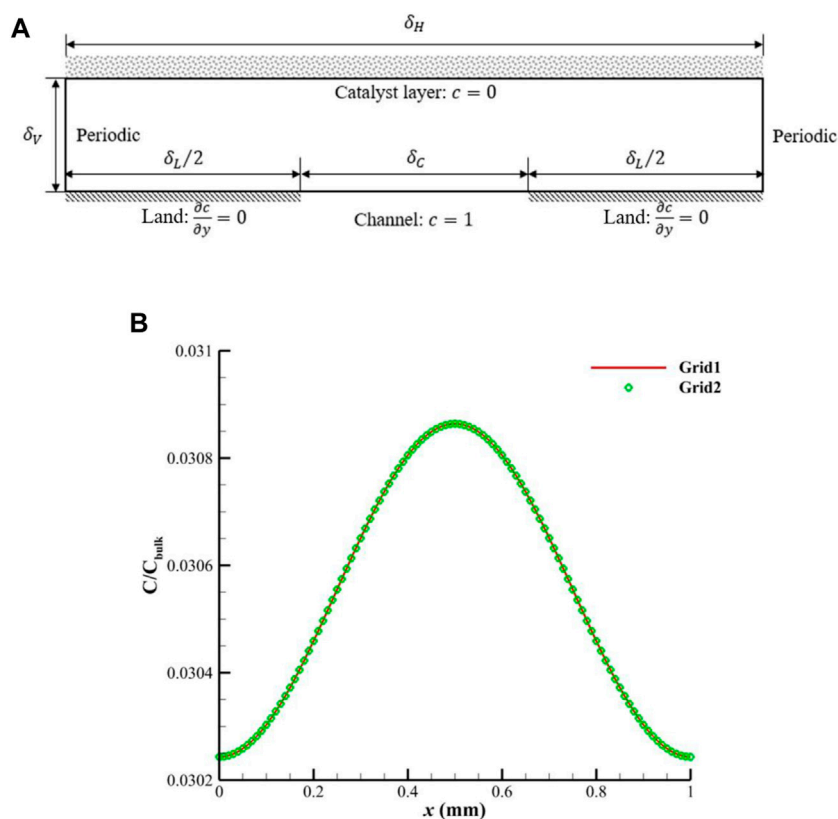


FIGURE 6 (A) Schematic representation of the numerical simulation region. (B) Distributions of oxygen concentration along the in-plane middle line on grids 1 and 2.

TABLE 3 Numerical conditions.

Case	Flow rate (ccm)	Torques (Nm)	δ_V (mm)	δ_H (mm)	$D_{H,apparent}$ (cm ² /s)	$D_{V,apparent}$ (cm ² /s)
1	2,000	2	0.21	0.5	1.17039	0.0727
2	1,800	2	0.21	0.5	0.90513	0.0830
3	1,400	2	0.21	0.5	0.50062	0.0552
4	1,000	2	0.21	0.5	0.26639	0.0545
5	600	2	0.21	0.5	0.12033	0.0176
6	200	2	0.21	0.5	0.06281	0.0244
7	2,000	2	0.21	1	1.17039	0.0727
8	2,000	3	0.21	0.5	0.2698	0.0727
9	2,000	4	0.21	0.5	0.09082	0.0727
10	2,000	5	0.21	0.5	0.05298	0.0727
11	2,000	6	0.21	0.5	0.02547	0.0727

simulation results under various torques with $\delta_c = 0.5$ mm. As the torque increases, the diffusion of oxygen in the land part of the GDL becomes increasingly difficult.

Figure 9 displays the distribution of the oxygen flux ratio (j/C_{bulk}) at the interface between GDL and catalyst layer under a gas

flow rate of 2,000 ccm. This ratio is linearly related to the limiting current for oxygen reduction, without accounting for the gas diffusion resistance in other compartments of PEMFC. At a torque of 2 Nm, there is no significant difference in the oxygen distribution between the land and channel parts. However, as the

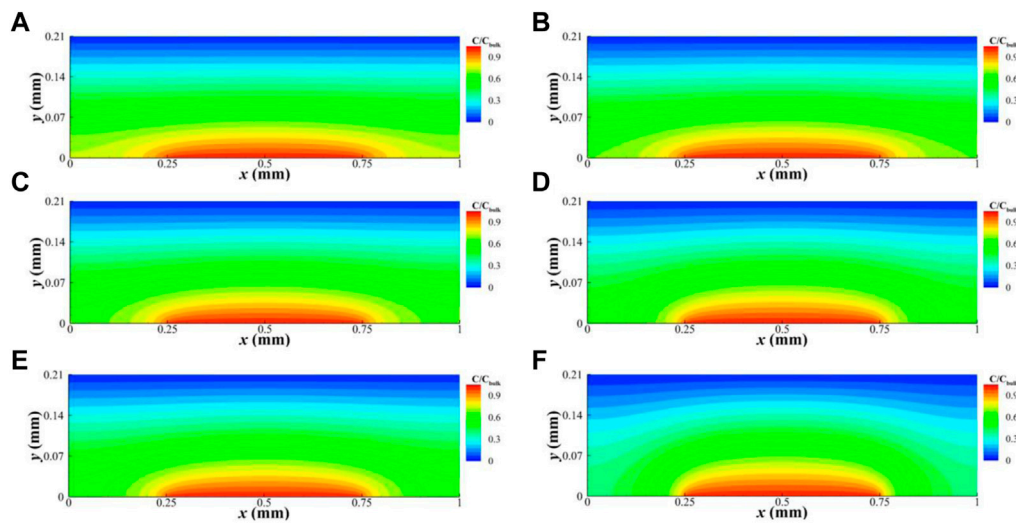


FIGURE 7 Oxygen concentration distribution in the GDL at torques of 2 Nm and a gas flow rate of 2,000 ccm (A), 1800 ccm (B), 1,400 ccm (C), 1,000 ccm (D), 600 ccm (E), and 200 ccm (F) when land and channel widths are 0.5 mm.

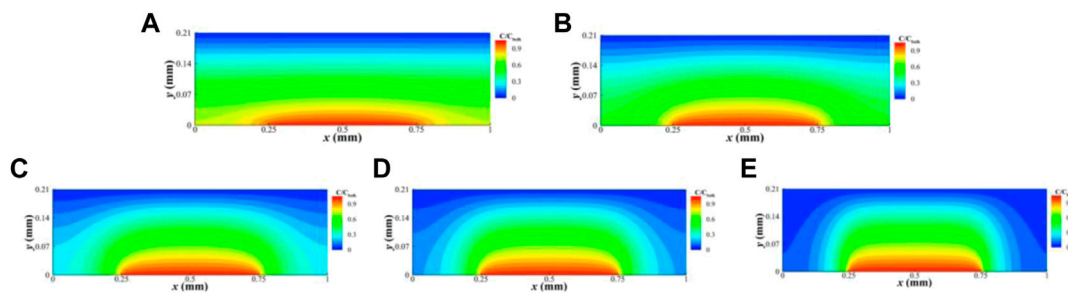


FIGURE 8 Oxygen concentration distribution in the GDL at a gas flow rate of 2000 ccm and torques of 2 Nm (A), 3 Nm (B), 4 Nm (C), 5 Nm (D), and 6 Nm (E) when land and channel widths are 0.5 mm.

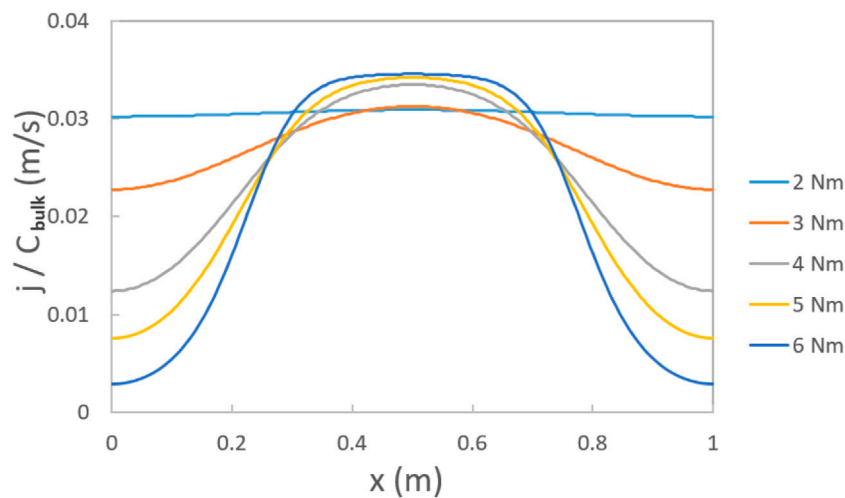


FIGURE 9 Ratio between the flux of O_2 (j) and O_2 bulk concentration (C_{bulk}) at the interface between the GDL and catalyst layer under torques of 2 Nm, 3 Nm, 4 Nm, 5 Nm, and 6 Nm with a land and channel width of 0.5 mm at gas flow rates of 2000 ccm (land part: $x = 0-0.25$ mm, $0.75-1$ mm; channel part: $x = 0.25-0.75$ mm).

torque increases from 2 to 6 Nm, the oxygen distribution in the land part decreases significantly. This suggests that smaller torques promote a more uniform distribution of oxygen in the GDL, as well as the current distribution in the PEMFC, without considering the influence on the contact resistance.

4 Conclusion

In this study, we developed methods for measuring and calculating the in-plane and through-plane oxygen apparent diffusion coefficients in GDL, using commercial carbon paper GDL (AvCarb EP40) as a case study. We found that both the in-plane and through-plane oxygen diffusion coefficients are affected by gas flow rates and torques. As the torque increases and the gas flow rate decreases, the in-plane oxygen diffusion coefficient decreases. We also simulated the oxygen flux distributions in GDL under various torques and gas flow rates. The results show that the channel part contributes to the majority of the oxygen flux, while the land part contribution decreases significantly with increasing torque. Overall, our results provide insights into the impact of torques and gas flow rates on the oxygen diffusion in fuel cells. This work may guide future studies on optimizing the design and operation of fuel cells for improved performance.

Data availability statement

The original contributions presented in the study are included in the article/Supplementary Material; further inquiries can be directed to the corresponding authors.

References

- Ahmed, D. H., and Sung, H. J. (2006). Effects of channel geometrical configuration and shoulder width on PEMFC performance at high current density. *J. Power Sources* 162, 327–339. doi:10.1016/j.jpowsour.2006.06.083
- Astrath, N. G. C., Shen, J., Song, D. T., Rohling, J. H., Astrath, F. B. G., Zhou, J. Q., et al. (2009). The effect of relative humidity on binary gas diffusion. *J. Phys. Chem. B* 113, 8369–8374. doi:10.1021/jp900796w
- Baker, D. R., Wieser, C., Neyerlin, K. C., and Murphy, M. W. (2006). The use of limiting current to determine transport resistance in PEM fuel cells. *ECS Trans.* 3, 989–999. doi:10.1149/1.2356218
- Beuscher, U. (2006). Experimental method to determine the mass transport resistance of a polymer electrolyte fuel cell. *J. Electrochem. Soc.* 153, A1788. doi:10.1149/1.2218760
- Chan, C., Zamel, N., Li, X. G., and Shen, J. (2012). Experimental measurement of effective diffusion coefficient of gas diffusion layer/microporous layer in PEM fuel cells. *Electrochim. Acta* 65, 13–21. doi:10.1016/j.electacta.2011.12.110
- Curtin, D. E., Lousenberg, R. D., Henry, T. J., Tangeman, P. C., and Tisack, M. E. (2004). Advanced materials for improved PEMFC performance and life. *J. Power Sources* 131, 41–48. doi:10.1016/j.jpowsour.2004.01.023
- Dai, W., Wang, H. J., Yuan, X. Z., Martin, J. J., Luo, Z. P., and Pan, M. (2008). Measurement of the water transport rate in a proton exchange membrane fuel cell and the influence of the gas diffusion layer. *J. Power Sources* 185, 1267–1271. doi:10.1016/j.jpowsour.2008.07.033
- Fluckiger, R., Freunberger, S. A., Kramer, D., Wokaun, A., Scherer, G. G., and Buchi, F. N. (2008). Anisotropic, effective diffusivity of porous gas diffusion layer materials for PEFC. *Electrochim. Acta* 54, 551–559. doi:10.1016/j.electacta.2008.07.034
- Khetabi, E., Bouziane, K., Zamel, N., Francois, X., Meyer, Y., and Candusso, D. (2019). Effects of mechanical compression on the performance of polymer electrolyte fuel cells and analysis through *in-situ* characterisation techniques - a review. *J. Power Sources* 424, 8–26. doi:10.1016/j.jpowsour.2019.03.071
- Kramer, D., Freunberger, S. A., Fluckiger, R., Schneider, I. A., Wokaun, A., Buchi, F. N., et al. (2008). Electrochemical diffusimetry of fuel cell gas diffusion layers. *J. Electroanal. Chem.* 612, 63–77. doi:10.1016/j.jelechem.2007.09.014
- LaManna, J. M., and Kandlikar, S. G. (2011). Determination of effective water vapor diffusion coefficient in pemfc gas diffusion layers. *Int. J. Hydrogen Energ.* 36, 5021–5029. doi:10.1016/j.ijhydene.2011.01.036
- Marrero, T. R., and Mason, E. A. (1972). Gaseous diffusion coefficients. *J. Phys. Chem. Reference Data* 1, 3–118. doi:10.1063/1.3253094
- Omrani, R., and Shabani, B. (2019). Review of gas diffusion layer for proton exchange membrane-based technologies with a focus on unitised regenerative fuel cells. *Int. J. Hydrogen Energ.* 44, 3834–3860. doi:10.1016/j.ijhydene.2018.12.120
- Ozden, A., Shahgaldi, S., Li, X. G., and Hamdullahpur, F. (2019). A review of gas diffusion layers for proton exchange membrane fuel cells-With a focus on characteristics, characterization techniques, materials and designs. *Prog. Energy Combust.* 74, 50–102. doi:10.1016/j.pecs.2019.05.002
- Rashapov, R., Imami, F., and Gostick, J. T. (2015). A method for measuring in-plane effective diffusivity in thin porous media. *Int. J. Heat. Mass Tran* 85, 367–374. doi:10.1016/j.ijheatmasstransfer.2015.01.101
- Rohling, J. H., Shen, J., Wang, C., Zhou, J., and Gu, C. E. (2007). Determination of binary diffusion coefficients of gases using photothermal deflection technique. *Appl. Phys. B-Lasers O.* 87, 355–362. doi:10.1007/s00340-007-2595-9
- Shen, J., Zhou, J., Astrath, N. G., Navessin, T., Liu, Z. S., Lei, C., et al. (2011). Measurement of effective gas diffusion coefficients of catalyst layers of PEM fuel cells with a Loschmidt diffusion cell. *J. Power Sources* 196, 674–678. doi:10.1016/j.jpowsour.2010.07.086
- Stumper, E., Lohr, M., and Hamada, S. (2005). Diagnostic tools for liquid water in PEM fuel cells. *J. Power Sources* 143, 150–157. doi:10.1016/j.jpowsour.2004.11.036
- Williams, M. V., Begg, E., Bonville, L., Kunz, H. R., and Fenton, J. M. (2004). Characterization of gas diffusion layers for PEMFC. *J. Electrochem. Soc.* 151, A1173. doi:10.1149/1.1764779
- Zamel, N., Astrath, N. G., Li, X., Shen, J., Zhou, J., Astrath, F. B., et al. (2010). Experimental measurements of effective diffusion coefficient of oxygen-nitrogen mixture in PEM fuel cell diffusion media. *Chem. Eng. Sci.* 65, 931–937. doi:10.1016/j.ces.2009.09.044

Author contributions

KY, TL, YaW, X-ZY, YY, and HW contributed to the conception and design of the study. KY wrote the first draft of the manuscript. All authors contributed to the article and approved the submitted version.

Funding

This work was supported by the Ministry of Education Key Laboratory of Energy Conversion and Storage Technologies (Y01406010), the Guangdong Innovative and Entrepreneurial Research Team Program (2016ZT06N500), and the Guangdong Provincial Key Laboratory of Energy Materials for Electric Power (2018B030322001).

Conflict of interest

The authors declare that the research was conducted in the absence of any commercial or financial relationships that could be construed as a potential conflict of interest.

Publisher's note

All claims expressed in this article are solely those of the authors and do not necessarily represent those of their affiliated organizations, or those of the publisher, the editors, and the reviewers. Any product that may be evaluated in this article, or claim that may be made by its manufacturer, is not guaranteed or endorsed by the publisher.